# Estudos em Ciências Exatas e da Terra

## Desafios, Avanços e Possibilidades

Alireza Mohebi Ashtiani
(organizador)

VOL III

EDITORA ARTEMIS
2025

# Estudos em Ciências Exatas e da Terra

## Desafios, Avanços e Possibilidades

Alireza Mohebi Ashtiani
(organizador)

VOL III

EDITORA ARTEMIS
2025

| | |
|---|---|
| **Editora Chefe** | Profª Drª Antonella Carvalho de Oliveira |
| **Editora Executiva** | M.ª Viviane Carvalho Mocellin |
| **Direção de Arte** | M.ª Bruna Bejarano |
| **Diagramação** | Elisangela Abreu |
| **Organizador** | Prof. Dr. Alireza Mohebi Ashtiani |
| **Imagem da Capa** | Abstract Style Landscapes /123RF |
| **Bibliotecário** | Maurício Amormino Júnior – CRB6/2422 |



Editora Artemis
Curitiba-PR Brasil
www.editoraartemis.com.br
e-mail:publicar@editoraartemis.com.br


Editora Artemis
Curitiba-PR Brasil
www.editoraartemis.com.br
e-mail:publicar@editoraartemis.com.br

**Dados Internacionais de Catalogação na Publicação (CIP)**
**(eDOC BRASIL, Belo Horizonte/MG)**

E82 Estudos em Ciências Exatas e da Terra: Desafios, Avanços e Possibilidades III / Organizador Alireza Mohebi Ashtiani. – Curitiba, PR: Artemis, 2025.

Formato: PDF
Requisitos de sistema: Adobe Acrobat Reader
Modo de acesso: World Wide Web
Inclui bibliografia
Edição bilíngue
ISBN 978-65-81701-75-8
DOI 10.37572/EdArt_101225758

1. Ciências exatas e da terra – Pesquisa – Brasil. I. Ashtiani, Alireza Mohebi.

CDD 509

**Elaborado por Maurício Amormino Júnior – CRB6/2422**

EDITORA ARTEMIS
2025

Editora Artemis
Curitiba-PR Brasil
www.editoraartemis.com.br
e-mail:publicar@editoraartemis.com.br

## PRÓLOGO

O volume III de **Estudos em Ciências Exatas e da Terra: Desafios, Avanços e Possibilidades** reúne um conjunto plural de pesquisas que refletem a vitalidade, a complexidade e o caráter interdisciplinar das ciências contemporâneas. Os dez capítulos aqui apresentados, provenientes de diversos países e contextos institucionais, oferecem um panorama abrangente dos desafios científicos atuais e das soluções inovadoras que emergem do diálogo entre matemática, física, química, engenharia, geociências, sustentabilidade ambiental e desenvolvimento territorial, reafirmando a amplitude teórica e aplicada dessas áreas.

Para favorecer a leitura e destacar as afinidades conceituais entre os temas, a obra foi organizada em três eixos temáticos que evidenciam os diferentes modos pelos quais o conhecimento científico se articula com problemas reais e necessidades sociais urgentes, propondo uma aproximação integradora e contemporânea das Ciências Exatas e da Terra.

**1. Modelagem Matemática, Simulação, Processos Físicos e Engenharia Aplicada**

O primeiro eixo reúne estudos orientados pela lógica da modelagem, da caracterização de materiais e da investigação de sistemas físico-químicos complexos. Aqui, a matemática desempenha um papel central, seja na descrição do crescimento populacional, na interpretação de curvas de relações molares ou na análise termoestrutural de concretos refratários usados na indústria siderúrgica. A ênfase comum está na busca por métodos rigorosos de análise, na construção de modelos interpretativos e na compreensão dos comportamentos materiais sob diferentes condições. Esses capítulos mostram como a formulação matemática e a experimentação se complementam, de forma decisiva, na explicação de fenômenos fundamentais para a ciência e a engenharia, evidenciando a potência dos métodos quantitativos na resolução de problemas complexos.

**2. Sustentabilidade, Meio Ambiente, Tecnologias de Remediação e Ecodesign**

O segundo eixo destaca pesquisas alinhadas aos desafios ambientais contemporâneos, trazendo propostas inovadoras para o desenvolvimento de tecnologias limpas, novos materiais sustentáveis e soluções de remediação ecológica. Os capítulos abordam desde práticas de ecodesign em produtos plásticos, passando pela criação de adsorventes de origem agroindustrial, até aplicações de biomassa vegetal para remoção de contaminantes e estratégias que ampliam o desempenho energético de sistemas fotovoltaicos, articulando ciência de materiais e preocupações ambientais. O núcleo

unificador deste eixo é o compromisso com a sustentabilidade, com a valorização de resíduos, com a mitigação de impactos ambientais e com a promoção de alternativas tecnológicas responsáveis e acessíveis que dialogam diretamente com demandas sociais emergentes.

**3. Território, Geociências e Desenvolvimento Agrário-Industrial**

O terceiro eixo aborda temas relacionados à organização do espaço, à história das indústrias de base e às dinâmicas socioeconômicas ligadas ao uso da terra. Os capítulos discutem a trajetória de figuras marcantes das geociências, analisam políticas e práticas de consolidação fundiária em escala nacional e refletem sobre as transformações industriais que moldam setores-chave como o agrícola e o petrolífero. Ao articular perspectivas históricas, econômicas e territoriais, este eixo evidencia como as ciências exatas e da terra também se expressam na compreensão dos processos sociais e produtivos que estruturam países e regiões, demonstrando que a pesquisa científica contribui igualmente para interpretações críticas sobre o desenvolvimento nacional.

A estrutura temática proposta pretende, portanto, facilitar a leitura e realçar o alcance multidisciplinar das pesquisas reunidas. Cada eixo demonstra, a seu modo, como o rigor científico pode contribuir para o entendimento de problemas concretos e para o desenvolvimento de soluções inovadoras, sejam elas de caráter teórico, tecnológico ou socioambiental, reforçando o papel estratégico da ciência na construção de futuros possíveis.

Esperamos que esta obra inspire pesquisadores, estudantes e profissionais a aprofundar o diálogo entre diferentes áreas do conhecimento e a reconhecer, na diversidade temática aqui apresentada, novas possibilidades de investigação e ação.

Desejo a todos uma excelente leitura!

Alireza Mohebi Ashtiani

## SUMÁRIO

## MODELAGEM MATEMÁTICA, SIMULAÇÃO, PROCESSOS FÍSICOS E ENGENHARIA APLICADA

## SUSTENTABILIDADE, MEIO AMBIENTE, TECNOLOGIAS DE REMEDIAÇÃO E ECODESIGN

TERRITÓRIO, GEOCIÊNCIAS E DESENVOLVIMENTO AGRÁRIO-INDUSTRIAL

# CAPÍTULO 1

## THERMOSTRUCTURAL BEHAVIOR OF A REFRACTORY CONCRETE FOR LADLE FURNACE[1]

*Data de submissão: 24/11/2025*
*Data de aceite: 08/12/2025*

**Edgardo Benavidez**
Universidad Tecnológica Nacional
Facultad Regional San Nicolás
San Nicolás de los Arroyos
Buenos Aires, Argentina
https://orcid.org/0000-0003-1524-4203

**ABSTRACT:** The structural development of an alumina ($Al_2O_3$) and spinel ($MgO{\cdot}Al_2O_3$) refractory concrete was evaluated at service temperatures (1000–1600 °C). This material, used in the steel industry, is part of the refractory lining of ladle furnaces. For the study, concrete specimens were cast and cured under ambient temperature and humidity conditions, then dried (105 °C – 24 h) and heat-treated (500 °C – 3 h). Structural variation was analyzed through dilatometry at a constant heating rate (5 °C/min up to 1600 °C) and isothermal dilatometry (4 hours) in the range of 1000–1500 °C. Specimens treated between 1000 °C and 1200 °C showed $Al_2O_3$ and $MgAl_2O_4$ as the main phases, while the formation of calcium hexaluminate ($CA_6$) was observed starting at 1400 °C. Dilatometry indicates that the refractory expands linearly up to around 1100 °C, then accelerates its expansion until approximately 1325 °C, a phenomenon associated with the formation of calcium dialuminate ($CA_2$). A contraction stage of the concrete occurs between 1330–1460 °C due to the sintering of ceramic grains; this densification behavior is slowed around 1460 °C by the increasing kinetics of calcium hexaluminate ($CA_6$) formation. From 1540 °C onward, the ceramic sintering process becomes dominant, leading to densification (contraction) of the material. Considering its specific use on the bottom or sidewall of a ladle furnace, and taking into account the different dimensional variations obtained in the isothermal dilatometry tests, the presence of compressive stresses is estimated in regions at temperatures between 1200 °C and 1300 °C, relative to zones at 1000 °C (considered neutral), and tensile stresses in refractory regions exposed to 1500 °C.
**KEYWORDS:** alumina; spinel; refractory; dilatometry; XRD.

### 1. INTRODUCTION

Conventional steel products are mainly manufactured through the integrated Blast Furnace process, followed by the primary metallurgy stage, which is commonly carried out in a vessel known as LD converter or Basic Oxygen Furnace (BOF). The steel is

[1] The author acknowledges the financial support provided by the National Technological University (Argentina) and the technical collaboration of Eng. Ricardo Ponte and Eng. Ailén Ponte. There are no conflicts of interes.

then transferred to ladle furnaces (LF) during the so-called secondary metallurgy stage, where the obtained steel undergoes an additional refining process (**Ghosh, 2001**). At this stage, the final adjustment of impurities in the liquid steel (sulfur, phosphorus, carbon, oxygen, nitrogen, and hydrogen) is performed, achieving a very low level of inclusions. This steel refining operation generally consists of deoxidation, desulfurization, and dephosphorization processes, through which controlled additions of alloying elements are made along with simultaneous modification of inclusions. These operations determine the type of refractory lining for the vessel.

The ladle lining uses carbon-containing refractory bricks, such as MgO-C (magnesia-carbon), $Al_2O_3$-MgO-C (alumina-magnesia-carbon), and CaO-MgO-C (dolomite-carbon). However, the need to produce ultra-low carbon content (ULCC) steels for automotive quality led to the use of carbon-free refractories to prevent carbon absorption from the lining (**Biswas & Sarkar, 2020**). Thus, alumina-spinel refractories ($Al_2O_3$-MgO·$Al_2O_3$) began to be used in ladle furnaces, particularly in wall areas in contact with molten metal (metal line) and in the bottom zone. At the ladle bottom (Fig. 1), the liquid metal directly impacts the refractory when steel is transferred from the converter to the ladle furnace, subjecting this type of castable to severe thermal and mechanical stresses.

The thickness of these refractories placed on the ladle bottom is around 300 mm. Therefore, during operation, this material is in direct contact with liquid steel, enduring temperatures of approximately 1600°C on its hot face and below 1000°C on its cold face. Consequently, the temperature gradient imposed on this material during service can generate different crystallographic phases throughout its thickness, considering that it is applied at low temperature and achieves consolidation upon being put into service. The formation of these phases is associated with volume changes, leading to the generation of mechanical stresses, mainly during the first hours of operation.

Fig. 1: Ladle furnace scheme.

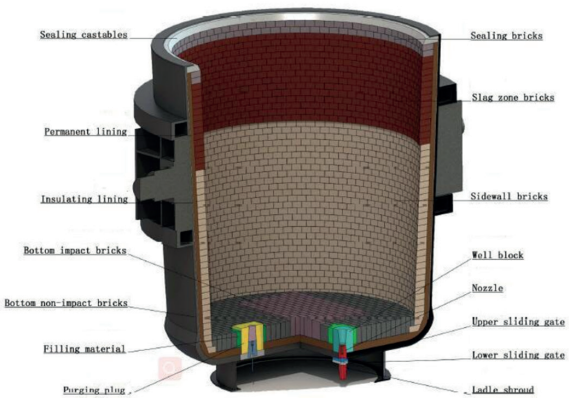

Alumina-spinel refractories are manufactured using synthetic aggregates of very high-purity alumina, such as white tabular alumina and white fused alumina, in addition to magnesium spinel (MA: $MgO{\cdot}Al_2O_3$), magnesia (MgO), and calcined alumina in fine fractions. High-alumina refractories with spinel addition offer advantages such as lower thermal conductivity and lower thermal expansion coefficient compared to MgO-C or $Al_2O_3$-MgO-C (AMC) bricks, resulting in reduced heat loss through the ladle wall, lower shell temperature, and high thermal shock resistance. Spinel (MA) can be added as "preformed" or can develop "in situ" in high-alumina castables during heating at high temperatures (**Zhang & Lee, 2004**). Refractories with preformed spinel exhibit high volumetric stability, while those with in-situ spinel have the advantage of gradual volumetric expansion with increasing temperature and high corrosion resistance against steel slags containing FeO and MnO (**Braulio et al., 2011**). Thus, preformed spinel is added to high-alumina castables for the following purposes: (i) to increase slag corrosion resistance and (ii) to improve high-temperature mechanical strength.

Moreover, MA spinel presents a stoichiometric range where the solid solubility of alumina in MA is greater than that of magnesia at the same temperature; therefore, alumina-rich MA spinels are commonly used in refractory manufacturing. In these cases, the notation $MgO{\cdot}nAl_2O_3$ is used, where n is the number of moles of alumina and can reach a value of n = 7.3 (**Jing et al., 2000**). The use of preformed spinel improves the mechanical strength of $Al_2O_3$–MA castables (**MacZura et al., 1995; Ko et al., 1994; Ko & Chan, 1999**). This improvement has been attributed to the reaction of CaO with alumina from alumina-rich MA, forming calcium hexaluminate ($CA_6$), which enhances bonding between spinel, alumina, and $CA_6$ grains in the matrix. The addition of alumina-rich spinel has also been shown to improve creep resistance in low- and ultra-low-cement alumina-spinel castables (**McConnell et al., 2002**). Thermo-mechanical properties of castables, such as hot modulus of rupture (HMOR) and refractoriness under load (RUL) of high-alumina refractories, are significantly improved by adding high-purity preformed spinel (**Sako et al., 2010**). Refractories with preformed spinel exhibit good thermal shock resistance and erosion resistance in applications such as purging plugs and well blocks used in steelmaking ladles (**Biswas & Sarkar, 2020**).

## 2. MATERIALS AND METODOLOGY

The material studied is an alumina-spinel castable that contains "preformed" spinel. The composition, as oxide percentages, is shown in Table 1.

Table 1: Composition (wt% of oxides) of the starting castable.

| **Oxide** | $Al_2O_3$ | $SiO_2$ | $Fe_2O_3$ | $Na_2O$ | MgO | CaO |
|---|---|---|---|---|---|---|
| **Wt.%** | 91.7 | 0.1 | 0.1 | 0.2 | 5.4 | 2.5 |

The castable used as the study material consists mainly of $Al_2O_3$, MgO, and CaO, with impurities (less than 0.2%) of $SiO_2$, $Fe_2O_3$, and $Na_2O$. Based on its CaO content (2.5 wt%), it can be classified as a low-cement castable. Considering the alumina percentage in ideal spinel (71.7% $Al_2O_3$ – 28.3% MgO), the material should have an alumina/spinel ratio of approximately 3. As shown later, the spinel incorporated in the starting material is an alumina-rich spinel. It is important to note that spinel is predominantly added to the fine fraction of the refractory castable.

Before shaping, the material was sieved to select particle sizes smaller than 6.35 mm (passing ASTM 1/4" mesh) to properly prepare the specimens for dilatometry. Prismatic castable specimens measuring 10 mm × 10 mm × 40 mm were shaped by casting in acrylic molds, with an addition of 6 wt% water. Curing was carried out under ambient temperature and humidity conditions for 72 hours. The specimens were then demolded and dried at 100°C for 24 hours. Subsequently, they were heat-treated at a rate of 20°C/h up to 350°C (3 hours) and then at 30°C/h up to 500°C (3 hours) to complete hydration reactions (Fig. 2.a). The specimens obtained in this way are referred to as HC and are shown in the image in Fig. 2.b.

Fig. 2: (a) Heat treatment and (b) specimens obtained prior to dilatometry tests.

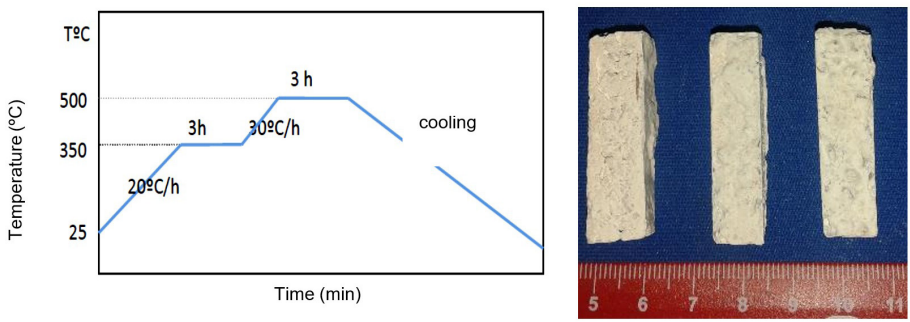


The HC specimens were subjected to different cycles in a horizontal dilatometer (Theta, Dilatronic II) at a heating rate of 5°C/min. A first HC sample was monitored up to 1600°C without holding time (designated HS-1600), and then five dilatometry tests were performed up to defined temperatures (TD) of 1000°C, 1200°C, 1300°C, 1400°C, and 1500°C, with a holding time of 4 hours at each $T_D$; these specimens were designated as HS-1000, HS-1200, HS-1300, HS-1400, and HS-1500, respectively.

The specimens tested in the dilatometry cycles were sectioned into three parts. One part was selected to determine apparent density and porosity using the Archimedes method with distilled water as the immersion liquid. Another part was embedded in resin, ground with SiC papers, and polished with diamond paste (6, 3, and 1 μm), then examined by scanning electron microscopy and energy-dispersive spectroscopy (SEM-EDS) using a FEG-SEM Quanta 200 microscope. A third part was ground into powder for crystallographic analysis by X-ray diffraction (XRD) using a Philips X'Pert Pro instrument.

## 3. RESULTS AND ANALYSIS

The XRD patterns obtained from the samples dried at 100°C (HC) show peaks corresponding to alumina and spinel phases (Fig. 3).

Fig. 3: X-ray diffraction pattern of the sample HC (100 °C-24 h).

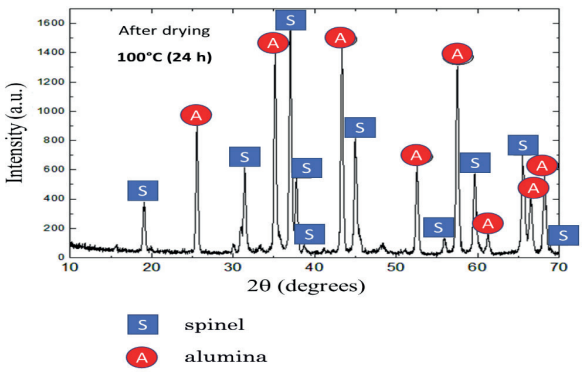


Table 2 lists the experimentally measured diffraction angles (2θ) for alumina and spinel and compares them with the theoretical values for both phases.

Table 2: Intensities of alumina and spinel peaks measured in the HC diffractogram.

**Alumina**

| 2θ (measured) | 2θ (theoretical) | Δ (2θ) |
|---|---|---|
| 25.53 | 25.576 | - 0.046 |
| 35.15 | 35.150 | 0.000 |
| 37.75 | 37.767 | - 0.017 |
| 43.37 | 43.340 | + 0.030 |
| 52.53 | 52.548 | - 0.018 |
| 57.51 | 57.498 | + 0.012 |
| 61.29 | 61.303 | - 0.013 |
| 66.55 | 66.514 | + 0.036 |
| 68.25 | 68.202 | + 0.048 |
| | | **+ 0.004°** |

**MA spinel**

| 2θ (measured) | 2θ (theoretical) | Δ (2θ) |
|---|---|---|
| 19.11 | 19.028 | + 0.082 |
| 31.43 | 31.270 | + 0.160 |
| 37.03 | 36.850 | + 0.180 |
| 38.73 | 38.522 | + 0.208 |
| 44.99 | 44.830 | + 0.160 |
| 55.91 | 55.656 | + 0.254 |
| 59.61 | 59.367 | + 0.243 |
| 65.53 | 65.238 | + 0.292 |
| 68.93 | 68.637 | + 0.293 |
| | | **+ 0.208°** |

It can be observed that the spinel peaks shift toward positive (2θ) values compared to those of stoichiometric spinel, whereas the alumina peaks do not. Considering Bragg's law:

$$\lambda = 2.d_{hkl}.sen\theta \quad (1)$$

where: λ = 1,54056 nm and $d_{hkl}$ is the interplanar spacing, and considering that magnesium spinel (MA) has a cubic structure, it is possible determine the lattice parameter (*a*) of MA spinel using the following expression:

$$d_{hkl} = \frac{a}{\sqrt{h^2 + k^2 + l^2}} \quad (2)$$

The lattice parameter of spinel reported in the literature (theoretical) and that obtained in this work (measured) are shown in Table 3.

Table 3: Calculation of the lattice parameter of MA from theoretical and experimental data.

| *h* | *k* | *l* | sin θ (theoretical) | *a* (Å) (theoretical) | sin θ (measured) | *a* (Å) (measured) |
|---|---|---|---|---|---|---|
| 1 | 1 | 1 | 0.165288596 | 8.0714 | 0.165994296 | 8.0374 |
| 2 | 2 | 0 | 0.269508133 | 8.0836 | 0.270852469 | 8.0438 |
| 3 | 1 | 1 | 0.316063032 | 8.0827 | 0.317552916 | 8.0451 |
| 2 | 2 | 2 | 0.329871891 | 8.0887 | 0.331584888 | 8.0472 |
| 4 | 0 | 0 | 0.381312409 | 8.0800 | 0.382602807 | 8.0531 |
| 4 | 2 | 2 | 0.466818872 | 8.0833 | 0.468777953 | 8.0498 |
| 5 | 1 | 1 | 0.4952085 | 8.0821 | 0.497049686 | 8.0525 |
| 4 | 4 | 0 | 0.539050123 | 8.0831 | 0.541194636 | 8.0514 |
| 5 | 3 | 1 | 0.563792755 | 8.0825 | 0.565902701 | 8.0527 |
| | | | | **0.8082 nm** | | **0.8048 nm** |

Thus, the lattice parameter determined for the spinel in the material under study is a = 0.805 nm, which is smaller than that calculated for stoichiometric spinel (0.808 nm). According to a previous study (**Jing et al., 2000**), where the variation of the spinel lattice parameter (a) was analyzed as a function of stoichiometry (n) for $MgO{\cdot}nAl_2O_3$, the value obtained is n = 1.4 (Fig. 4.a).

Fig. 4: (a) Spinel lattice parameter as a function of the number of alumina moles (n) in the MA stoichiometry and (b) its position in the $MgO\text{-}Al_2O_3$ diagram.

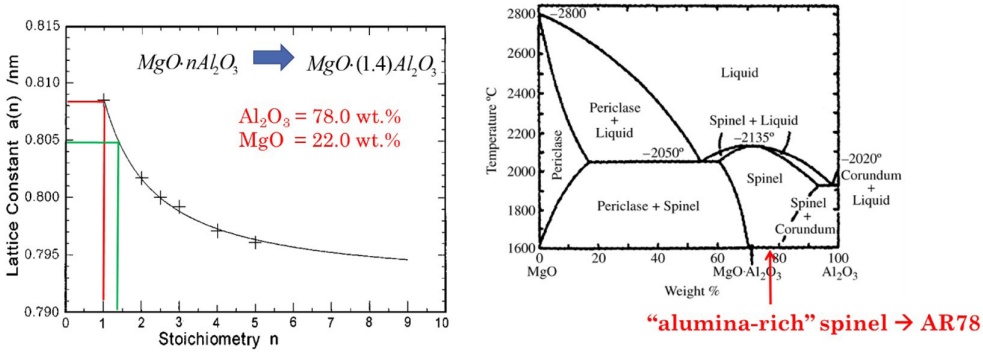


This MA stoichiometry corresponds to an alumina content of approximately 78 wt%, considering the $MgO\text{-}Al_2O_3$ phase equilibrium diagram (Fig. 4.b). Based on this result, it can be estimated that the spinel used as the raw material in the castable under study is an MA of the AR78 type.

The different crystalline phases detected in the HC specimens after the dilatometry tests are presented in Table 4.

Table 4: Crystalline phases observed in HS specimens at different temperatures.

| **Temperature** | **1000°C** (4 h) | **1200°C** (4 h) | **1300°C** (4 h) | **1400°C** (4 h) | **1500°C** (4 h) | **1600°C** (0 h) |
|---|---|---|---|---|---|---|
| Crystalline phases | A<br>MA<br>CA<br>$C_{12}A_7$ | A<br>MA<br>$CA_2$ | A<br>MA<br>$CA_2$ | A<br>MA<br>$CA_6$<br>$CA_2$ | A<br>MA<br>$CA_6$ | A<br>MA<br>$CA_6$ |

A = $Al_2O_3$
MA = $MgO \cdot Al_2O_3$
CA = $CaO \cdot Al_2O_3$
$CA_2$ = $CaO \cdot 2Al_2O_3$
$C_{12}A_7$ = $12CaO \cdot 7Al_2O_3$
$CA_6$ = $CaO \cdot 6Al_2O_3$

The diffractograms of HS specimens treated at 1400°C, 1500°C, and 1600°C are shown in Fig. 5.

Fig. 5: X-ray diffractograms of HS samples and percentages of phases present.

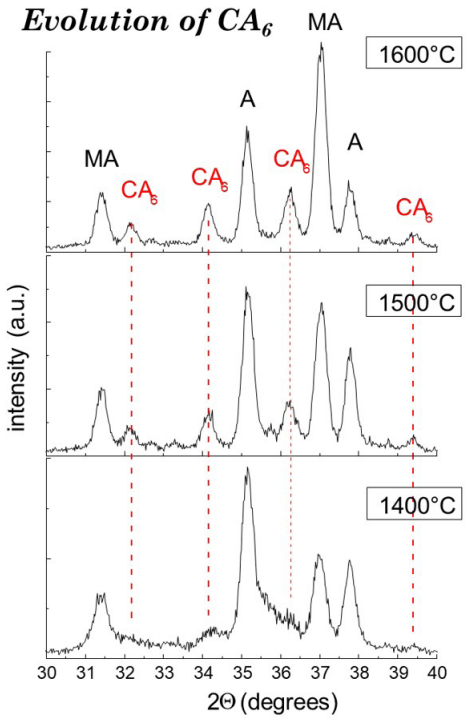


| Temp (°C) | % $Al_2O_3$ | % MA | A:MA |
|---|---|---|---|
| 1000 | 76 | 24 | ≈ 3,2 |
| 1200 | 74 | 26 | ≈ 2,8 |
| 1300 | 75 | 25 | ≈ 3,0 |
| 1400 | 77 | 23 | ≈ 3,3 |
| 1500 | 59 | 41 | ≈ 1,4 |
| 1600 | 53 | 47 | ≈ 1,1 |

| Temp (°C) | % $Al_2O_3$ | % MA | % $CA_6$ |
|---|---|---|---|
| 1500 | 53 | 33 | 14 |
| 1600 | 37 | 44 | 19 |

These diffractograms show the development of calcium hexaluminate ($CA_6$), which begins to appear at around 1400°C and then exhibits increasing peak intensity at 1500°C and 1600°C. The percentages calculated from the peak intensities of alumina (A), spinel (MA), and calcium hexaluminate (see tables to the right of the diffractograms) indicate the highest $CA_6$ content in the specimen treated at 1600°C. The reaction kinetics for $CA_6$ formation from $CA_2$ and $Al_2O_3$ is very slow at temperatures below 1350°C but increases significantly above 1450°C (**Pieta et al., 2015**).

On the other hand, performing a similar analysis on the alumina-to-spinel ratio (A:MA) reveals a decrease in the alumina percentage, which is associated with the consumption of $Al_2O_3$ due to the increased formation of $CA_6$.

Figure 6 shows micrographs (left) and EDS analyses (right) of different specimens.

Fig. 6: Micrographs of specimens and EDS analysis of the HC (top), HS-1200 (center), and HS-1400 (bottom) specimens.

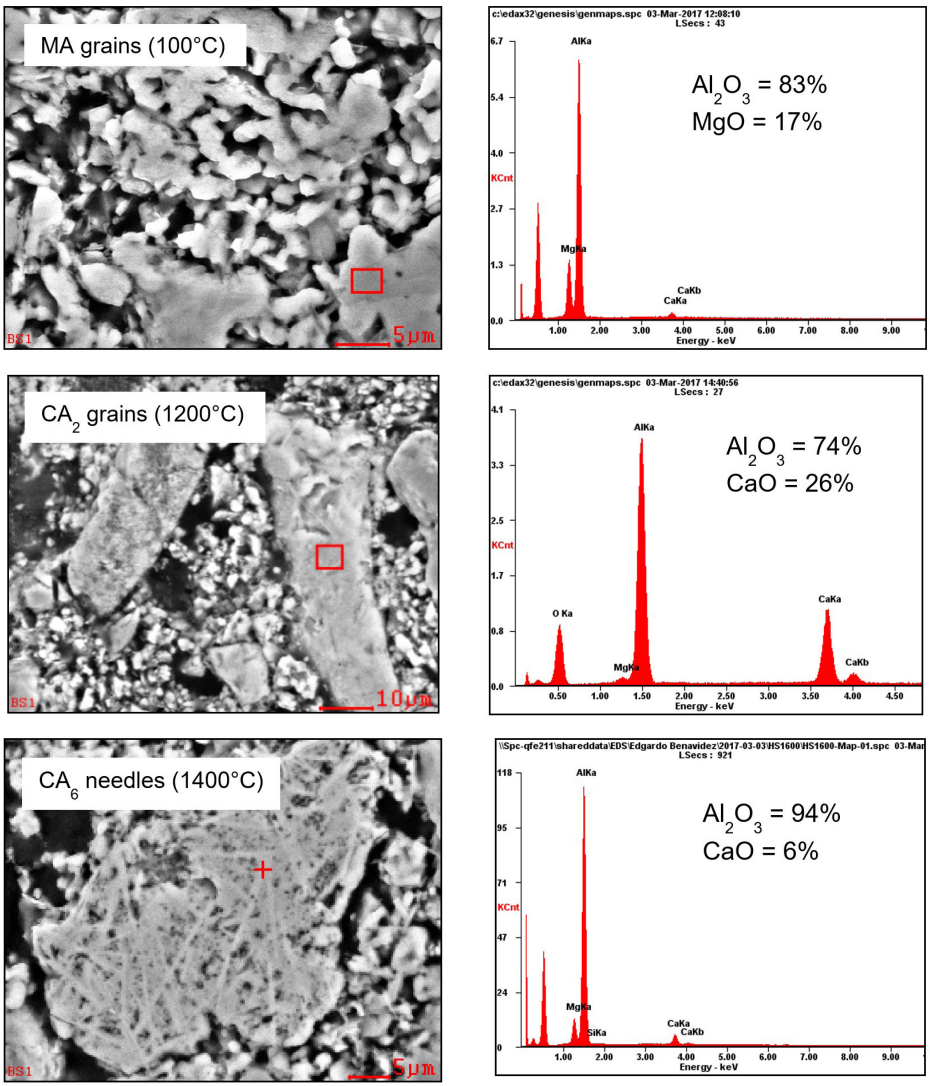


The top micrograph corresponds to the HC specimen (100°C – 24h), where MA spinel grains (red square) stand out, with a content of ≈83% $Al_2O_3$. Thus, through EDS analysis, it is established, consistent with the XRD peaks of this sample, that the MA spinel grains are rich in alumina. The center micrograph corresponds to the HS-1200 specimen, where calcium dialuminate ($CA_2$) grains (red square) are highlighted (see EDS spectrum). According to the values in Table 4, this phase is present at 1200, 1300, and 1400°C, later reacting with alumina (A) to form calcium hexaluminate ($CA_6$). In the bottom micrograph corresponding to the HS-1400 specimen, $CA_6$ “needles” (red cross) are highlighted.

The apparent porosity values determined for these specimens are shown in Fig. 7. The open porosity remains constant between 1000–1200°C (≈16 vol %), showing a significant increase at 1300°C, where the highest porosity is observed (≈ 25 vol %). The porosity values then decrease smoothly and continuously for HS-1400 (≈ 23 vol %) and HS-1500 (≈ 21 vol %).

Fig. 7: Open porosity values at different temperaturas.

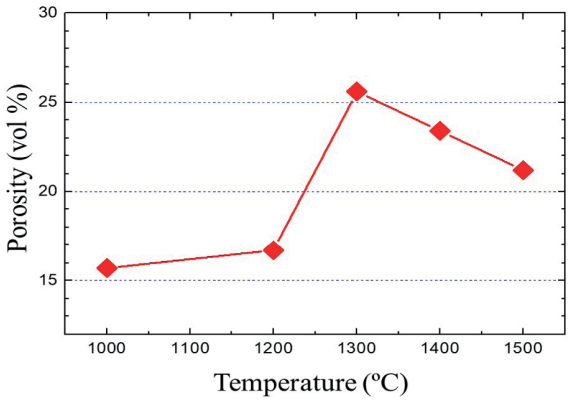


The lower porosity measured from 1400 °C onward may be associated with the formation of calcium hexaluminate ($CA_6$) at that temperature. According to some authors, $CA_6$ grains are detected inside the pores, preventing the formation of interconnected pores (**Wang et al., 2018**), which are directly linked to apparent porosity. In addition, the expansion of $CA_6$ grains tends to reduce pore size.

For the volumetric changes of the calcium–alumina (CA) phases, the values presented in Table 5 are considered, where the weight percentages of lime and alumina, melting temperature ($T_{melt}$), density (ρ), molar mass ($M_m$), and molar volume ($V_m$) of the different phases are listed, as considered in this work.

Table 5. Properties of CA phases.

| Mineral | $T_{melt}$ (°C) | CaO (%) | $Al_2O_3$ (%) | ρ (g/cm³) | $M_m$ (g/mol) | $V_m$ (cm³/mol) |
|---|---|---|---|---|---|---|
| C | 2570 | 100 | - | 3,32 | 56,08 | 16,89 |
| $C_{12}A_7$ | 1415-1495 | 48,6 | 51,4 | 2,69 | 1386,64 | 515,48 |
| CA | 1600 | 35,5 | 64,5 | 2,98 | 158,04 | 53,03 |
| $CA_2$ | 1750-1765 | 21,6 | 78,4 | 2,91 | 260,00 | 89,35 |
| $CA_6$ | 1830 | 8,4 | 91,6 | 3,38 | 667,84 | 197,59 |
| A | 2051 | - | 100 | 3,98 | 101,96 | 25,62 |

The general thermal behavior of the concrete up to 1600 °C is shown in Fig. 8 (**Benavidez et al., 2018**). It can be observed that the concrete expands linearly up to around 1100 °C; from that point, the curve accelerates its expansion until reaching 1325 °C. Then, the concrete begins to contract slowly until reaching 1385 °C. From this temperature onward, the contraction rate increases and stops around 1480 °C. At approximately 1530 °C, the contraction accelerates again until reaching 1620 °C, which is the maximum temperature recorded in the test.

Fig. 8: Dilatometric curve of concrete up to 1600 °C (HS-1600 specimen).

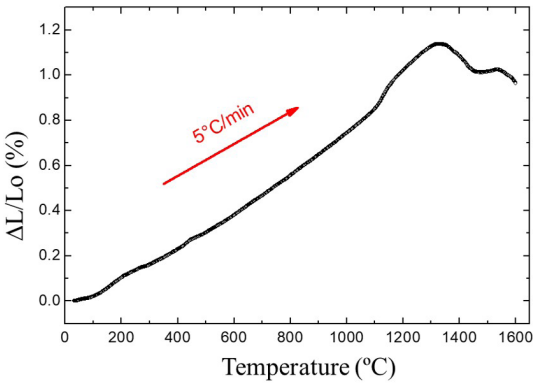


The area of interest in the dilatometric curve focuses on the region between 1000–1600 °C. Fig. 9 shows this region, where the material exhibits expansions and contractions within this temperature range, and four zones are identified. In zone (1), between 1110 °C and 1325 °C, an expansion is observed, which is attributed to the formation of calcium dialuminate through the reaction in Eq. 3, representing a volume increase of ≈ 13.5 % (**Wang et al., 2016**), according to the $M_m$ and $V_m$ values given in Table 5.

$$CA + A = CA_2 \quad (3)$$

Expansions due to the formation of $CA_2$ from CA and alumina have previously been reported (**Criado et al., 1976**). Zone (2), between 1330 °C and 1460 °C, shows a contraction attributed to the sintering of ceramic grains, which produces densification of the material. Zone (3), starting at 1460 °C, shows a slight expansion associated with the formation of $CA_6$, according to Eq. 4.:

$$CA_2 + 4A = CA_6 \quad (4)$$

This small volumetric expansion of ≈ 3 % (**Wang et al., 2016**) slows down the densification of the concrete in the range of 1480–1530 °C. In some cases, this expansion

has been attributed to the bonding between $CA_6$ grains and spinel grains in the matrix (**Ko and Lay, 2000**) or to the formation of hexagonal $CA_6$ platelets (**Auvray et al., 2008**). However, other authors have associated the reaction in Eq. (4) with a volume contraction (**Xu et al., 2015**).

Finally, from 1540 °C onward, zone (4), the sintering of ceramic grains once again dominates the densification of the material. At this stage, the presence of a small amount of liquid phase could also be expected, due to impurities in the raw materials, which may accelerate the sintering/densification of the refractory (**Ko and Lay, 2000**).

Fig. 9: Identification of the different zones of the HS-1600 dilatometric curve.

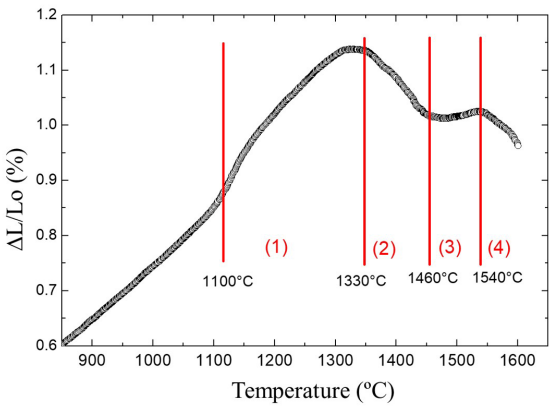


Fig. 10 shows, as an example, the isothermal dilatometry of HS-1300, where a constant heating rate of 5 °C/min is applied up to 1300 °C, maintaining that temperature for 4 hours.

Fig. 10: Dilatometric behavior of the sample HS-1300.

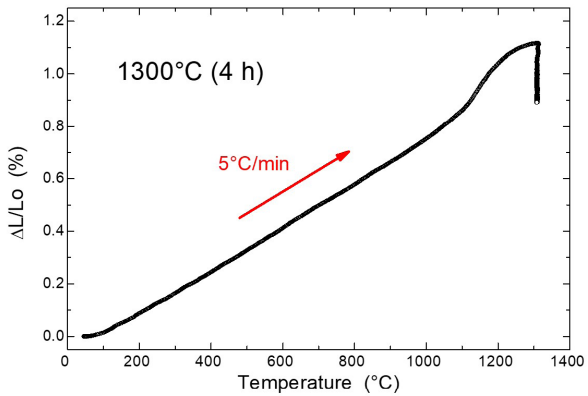


The isothermal dilatometries (4 hours) at the different $T_D$ are shown in Fig. 11. In these curves, $L_0$ is considered as the length of the specimen at temperature $T_D$.

The dilatometries show that at 1000 °C there is a slight expansion behavior of the specimen ($\Delta L/L_0 > 0$), while for the remaining TD, the behavior is contraction. The contraction values, starting from TD = 1200 °C, increase as the temperature rises.

Fig. 11: Isothermal behavior at different temperatures $T_D$.

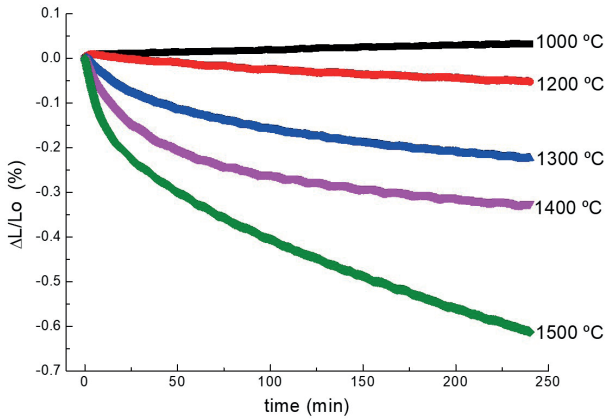


Table 6 lists the expansion and contraction values obtained at the different temperatures.

Tabla 6: Expansion and contraction values in isothermal dilatometry at different $T_D$.

| Temp (°C) | $\Delta L/L_o$ (%) | Behavior |
|---|---|---|
| 1000 | + 0.025 | expansion |
| 1200 | - 0.062 | contraction |
| 1300 | - 0.224 | contraction |
| 1400 | - 0.310 | contraction |
| 1500 | - 0.613 | contraction |

Considering a temperature gradient such as the one present in concrete located on a ladle floor, the dilatometry data indicate the presence of stresses resulting from the different dimensional changes. As mentioned, the refractory located at the bottom of the ladle is subjected to a temperature gradient ranging from 1600 °C on the hot face (in contact with the molten steel) to temperatures below 1000 °C on the cold face.

Analyzing the profile of contractions and expansions after 4 hours (Table 6), and considering a neutral stress at 1000 °C, a mechanical stress profile such as the one shown in Fig. 12 may be present in the alumina–spinel concrete analyzed in this work. The temperature of 1000 °C was selected as the point of neutral stress because, below this temperature, no significant dimensional variations are recorded. The $\Delta L/L_0$ (%) values

indicated on the dilatometric curve in Fig. 12 refer to the initial length ($L_0$) recorded at room temperature. This means that, relative to this initial $L_0$, the concrete will have an expansion of ≈ 0.77 % at 1000 °C (after 4 h), while it will have expanded ≈ 0.96 % at 1200 °C (4 h), ≈ 0.90 % at 1300 °C (4 h), ≈ 0.77 % at 1400 °C (4 h), and finally ≈ 0.40 % at 1500 °C (4 h).

Fig. 12: Compressive and tensile stresses developed at different temperature levels.

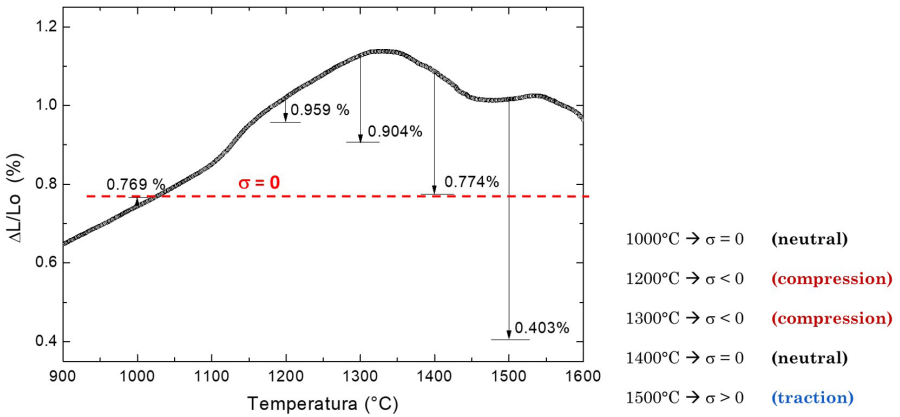


Thus, if applied stresses are not considered (as in dilatometry tests), the zones at 1200 °C and 1300 °C, after 4 hours, will reach greater expansions (0.959 % and 0.904 %, respectively) relative to the initial length ($L_0$) measured at room temperature. Therefore, the layers of concrete in service that register these temperatures tend to have a greater length than the zone at 1000 °C (taken as neutral), meaning that, in service, they would be subjected to compressive stresses ($\sigma < 0$).

Conversely, the region located at 1500 °C (4 h) shows an expansion value (0.403 %) lower than that at 1000 °C (0.769 %). Therefore, after 4 hours in service, the concrete zones situated at 1400 °C (near the hot face) will be subjected to tensile stresses ($\sigma > 0$) relative to the zone at 1000 °C (farther from the hot face). These zones under tensile stress can be considered prone to thermomechanical failure.

Finally, the region located at 1400 °C shows a linear expansion (0.774 %) of the same order as that obtained at 1000 °C (0.769 %), so mechanical stresses can be considered negligible ($\sigma = 0$) relative to the zone at 1000 °C.

## 4. CONCLUSIONS

Some key points to highlight in this study were: (i) the evolution of the crystalline phases of a commercial alumina–spinel concrete between 1000 °C and 1600 °C was determined; (ii) the dimensional changes associated with the formation of calcium

dialuminate and calcium hexaluminate were confirmed through porosity and dilatometry data; (iii) a profile of dimensional variations based on isothermal dilatometry data was presented. At this point, it is important to emphasize the generation of thermomechanical stresses due to the dimensional changes experienced by this material in a steel ladle, where a significant temperature gradient occurs under service conditions.

## REFERENCES


Auvray. J-M., Gault, C. y Huger, M. (2008). Microstructural changes and evolutions of elastic properties versus temperatura of alumina and alumina-magnesia refractory castables. *J. Eur. Ceram. Soc.*, *28*, 1953-1960.

Benavidez, E., Ponte, A. y Ponte R. (2018). Comportamiento térmico de un hormigón refractario para aplicaciones en horno cuchara. *Libro de resúmenes extendidos del 18° Congreso Internacional de Metalurgia y Materiales*. Bariloche, Argentina. 336-338.

Biswas, S. y Sarkar, D. (2020). Introduction to Refractories for Iron- and Steelmaking. Springer Nature. https://doi.org/10.1007/978-3-030-43807-4.

Braulio, M. A. L., Rigaud, M., Buhr, A. Parr, C. y Pandolfelli, V. C. (2011). Spinel-containing alumina-based refractory castables. *Ceram. Int.*, *37*, 1705-1724.

Criado, E., Estrada, D.A. y de Aza, S. (1976). Estudio dilatométrico sobre la formación de dialuminato y hexaluminato de calcio en cementos y hormigones refractarios. *Bol. Soc. Esp. Cerám. Vidr.*, *15*(5). 319-321.

Ghosh, A. (2000). *Secondary Steel Making – Principle and Applications*, CRC Press. DOI: 10.1201/9781420042313.

Jing, S.Y., Lin, L.B., Huang, N.K., Zhang, J. y Lu, Y (2000). Investigation on lattice constants of Mg-Al spinels. *J. Mater. Sci. Lett.*, *19*, 225–227.

Ko, Y-C. y Lay, J. T. (2000). Thermal expansion characteristics of alumina-magnesia and alumina-spinel castables in the temperature range 800-1650°C. *J. Am. Ceram. Soc. 83*, 2872-2874.

Ko, Y-C. y Chan, C. F. (1999). Effect of spinel content on hot strength of alumina-spinel castables in the temperature range 1000–1500°C. *J. Eur. Ceram Soc*, *19*, 2633–2639.

MacZura, G., Madono, M., Kriechbaum, G. W. y Sewell, B. (1995). Low moisture regular corundum/spinel castables with superior properties. Proc. Unified Intl. Tech. Conf. On Refractories, Kyoto, Japan, 179-186.

McConnell, R.W., Marra, R.A. y Fullington, F.A. (2002). Benefits of sintered magnesium aluminate spinels in high purity castable refractories. *Refractories Applications and News 7*(2), 23–28.

Pieta, A., Bucko, M. M., Janus, M., Lis, J. y Jonas, S. (2015). Calcium hexaluminate synthesis and its influence on the properties of $CA_2$-$Al_2O_3$-based refractories. *J. Eur. Ceram. Soc.*, *35*, 4567-4571.

Sako, E.Y., Braulio, M. A. L., Brant, P. O. y Pandolfelli, V. C. (2010). The impact of pre-formed and in-situ spinel formation on the physical properties of cement bonded high alumina refractory castables. *Ceram. Int.*, *36*, 2079–2085.

Vance, M.W., Kriechbaum, G.W., Henrichsen, R.A., MacZura, G., Moody, K.J. y Munding, S. (1994). Influence of spinel additives on high-alumina/spinel castables. *Bull. Am. Ceram. Soc.*, *73*, 70–74.

Wang, Q., Li, Y., Xu, N., Xiang, R. y Li, S. (2018). Microstructure and phase evolution of cement-bonded high-alumina refractory castables for porous purging plugs. *J. Ceram. Sci. Technol., 9*, 1-6.

Wang, Y., Li, X., Zhu, B. y Chen, P. (2016). Microstructure evolution during the heating process and its effect on the elastic properties of CAC-bonded alumina castables. *Ceram. Int*., *42*, 11355-11362.

Xu, L., Chen, M., Huang, W-J., Wang, N., Dong, J-H y Ying, X-L. (2015). Effects of CaO content on sintering and lightweight of $Al_2O_3$-MgO-CaO refractories. *Materials Research Innovations*, *19*, 212-217.

Zhang, S. y Lee, W. E. (2004). Spinel-Containing Refractories en C.A Schacht, (Ed.). *Refractories Handbook*. (pp. 215-257) Marcel Dekker Inc.

## SOBRE O ORGANIZADOR

Alireza Mohebi Ashtiani possui graduação em bacharelado em Matemática, Matemática Aplicada, pela Amirkabir University of Technology (Polytechnic of Tehran), Teerã/Irã (2003), mestrado em Matemática Aplicada pelo Institute for Advanced Studies in Basic Siences (IASBS), Zanjan/Irã (2005) e doutorado em Engenharia Elétrica pela Universidade Estadual de Campinas (UNICAMP) na área de Automação (2012). Foi bolsista de Pós-doutorado Júnior do CNPq no Instituto de Matemática, Estatística e Computação Científica (IMECC/UNICAMP) e bolsista de Pós-doutorado da Fundação de Amparo à Pesquisa do Estado de São Paulo (FAPESP) na Faculdade de Ciências Aplicadas da Universidade Estadual de Campinas (FCA/UNICAMP). Desde 2013 é docente vinculado ao Departamento Acadêmico de Matemática do Campus Londrina da Universidade Tecnológica Federal do Paraná (UTFPR), e atualmente, docente permanente do Programa de Pós-Graduação em Matemática em Rede Nacional (PROFMAT) da UTFPR, Campus Cornélio Procópio.

Alireza Mohebi Ashtiani
http://lattes.cnpq.br/5025709771742662

## ÍNDICE REMISSIVO

## X



## Y


EDITORA
ARTEMIS
2025